ACS APPLIED MATERIALS & INTERFACES

RESEARCH ARTICLE

www.acsami.org

Photocatalytic Activity of Heterostructures Based on TiO_2 and Halloysite Nanotubes

Rijing Wang,[†,‡] Guohua Jiang,[*,†,‡] Yuanwei Ding,[†,‡] Yin Wang,[†,‡] Xinke Sun,[†,‡] Xiaohong Wang,[†,‡] and Wenxing Chen[*,†,‡]

[†]Department of Materials Engineering, College of Materials and Textile, and [‡]Key Laboratory of Advanced Textile Materials and Manufacturing Technology (ATMT), Ministry of Education, Zhejiang Sci-Tech University, Hangzhou 310018, P. R. China

Supporting Information

ABSTRACT: A one-step solvothermal method was used to prepare TiO_2/halloysite composites. TiO_2 nanoparticles were deposited on the platform of the halloysite nanotubes (HNTs). XRD, FT-IR, FE-SEM, and TEM were applied to investigate the structures and morphologies of the resultant samples. The as-prepared TiO_2/HNTs photocatalyst exhibits pH sensibility on the degradation of methanol and a higher photocatalytic activity on the degradation of acetic acid. The combination of the photocatalytic property of TiO_2 and the unique structure of halloysite endowed this material with a bright perspective in degradation of organic pollutant.

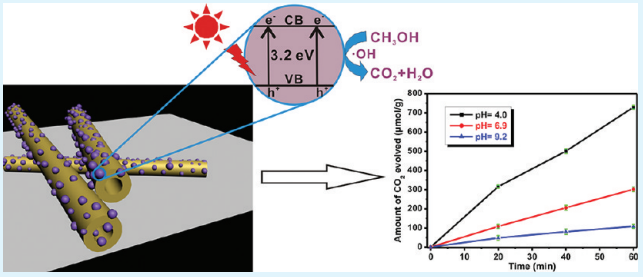

KEYWORDS: halloysite nanotubes, TiO_2, solvothermal method, photocatalyst

1. INTRODUCTION

With the rapid development of industry, the volume of wastewater and gas generated has increased significantly. To date, there is still not an effective way to purify the wastewater or gas. So it is urgent to develop a new technology that can be used to effectively address these issues. TiO_2 has been extensively used in a wide range of applications (such as gas sensor, solar cell, batteries and so on), since the discovery of its application in photocatalysis.[1−5] In particular, nanosize TiO_2 has attracted considerable attention in photocatalytic applications due to its unique properties such as quantum confinement and high surface to volume ratio.[6−9] However, TiO_2 nanoparticles are prone to aggregate, resulting in an adverse effect on the photocatalytic activity. Consequently, great efforts have been made to block the aggregation of TiO_2 nanoparticles, such as supported technology, coating method and so on.[10−12]

To date, there has been great interest in preparation of the supported catalysts, for instance, carbon nanotubes composites,[13−15] magnetic composites,[16,17] graphene composites,[18−20] etc., because of their enhanced photocatalytic activity or magnetic separation. Halloysite nanotubes (HNTs) are two-layered aluminosilicate clay and have exhibited promising results as a catalyst support because of their inherent hollow nanotube structure and different outside and inside chemistry.[21,22] Deposited the TiO_2 nanoparticles onto HNTs is a promising method to block their aggregation. Furthermore, HNTs possess advantages of high stability, resistibility against organic solvents and ease of disposal or reusability.[23] Compared to carbon nanotubes (CNTs), HNTs are an economically available raw material and have some unique characteristics, such as different outside and inside chemistry and adequate hydroxyl groups on the surface of HNTs.[24,25] Then HNTs can be directly used to support the TiO_2 nanoparticles because of these hydroxyl radicals. Therefore, the combination of TiO_2 and HNTs is promising to simultaneously possess excellent photocatalytic activity and adsorptivity, which could deliver exceptional performances in photocatalytic degradation of pollutants. Recently, Papoulis et al. have reported the fabrication of clay-supported TiO_2 composites by templating TiO_2 sol solutions on halloysite nanotubes and subsequently hydrothermal treatment.[26] To improve relevance for TiO_2/HNTs applications, the synthesis approach should be simple and effective.

Herein, a one-step solvothermal method was applied to prepare TiO_2/HNTs composites. TiO_2 nanoparticles were deposited on the surface of HNTs, as illustrated in Scheme 1. The TiO_2/HNTs simultaneously covered their excellent properties of TiO_2 and HNTs, exhibited high photocatalytic activity and pH sensibility, and endowed this material with a bright perspective in degradation of organic pollutant.

2. EXPERIMENTAL SECTIONS

2.1. Materials and Reagents. The halloysite nanotubes (HNTs) were obtained from Wenzhou Xincheng Shenfei Aluminum Alloy Co., Ltd., China. Pure TiO_2 was purchased from Degussa Co. Ltd., butyl

Received: August 1, 2011
Accepted: September 13, 2011
Published: September 14, 2011

Scheme 1. Schematic Structure of TiO_2/HNTs and the Photocatalytic Process over TiO_2 /HNTs

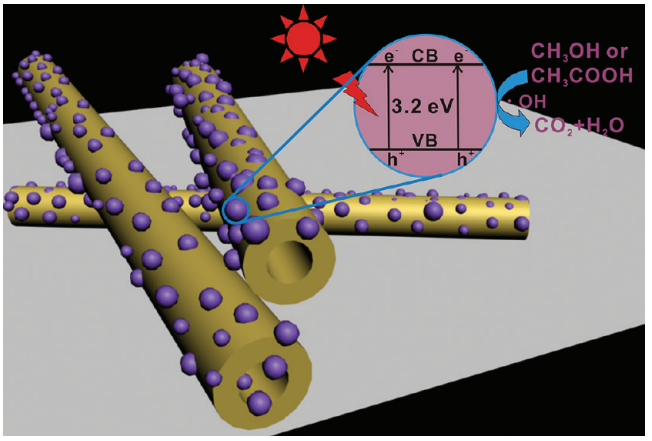

titanate and isopropanol were purchased from Shanghai Chemical Co., Ltd. All reagents were analytical grade and used without further purification.

2.2. Preparation of TiO_2/Halloysite Nanotube Composites. In the typical preparation, butyl titanate (2 mL) was dissolved in 40 mL of isopropanol to obtain the precursor solution. Then the halloysite nanotubes (1 g) were added to the above solution under constant stirring, and the pH of solution was adjusted to 4 by hydrochloric acid (0.1 M). Next, the resultant solution transferred into a Teflon-lined stainless steel autoclave, followed by a solvothermal treatment at 160 °C for 24 h. After cooled to room temperature, the precipitates were washed with deionized water and ethanol five times and dried in a vacuum oven at 60 °C for 12 h. At last, the TiO_2/HNTs composite containing 31.8 wt % TiO_2 was obtained.

2.3. Characterization. The morphology and microstructure of TiO_2/HNTs were analyzed with a SIEMENS Diffraktometer D5000 X-ray diffractometer using Cu Kα radiation source at 35 kV, with a scan rate of 0.02° 2θ s^{-1} in the 2θ range of 10−70°, ULTRA-55 field-emission scanning electron microscopy (FE-SEM) and transmission electron microscopy (TEM) (JSM-2100) equipped with an energy dispersive X-ray spectrum (EDS, Inca Energy-200) at an accelerating voltage of 200 kV. Fourier transform infrared (FT-IR) spectra were recorded on a Nicolet 5700 spectrophotometer using KBr pellets for samples. The Brunauer−Emmet−Teller (BET) specific surface area of the samples were determined by a high speed automated area and pore size analyzer (F-Sorb3400, China).

2.4. Measurement of Photocatalytic Activity. The photocatalytic activity of TiO_2/HNTs was investigated by the photodegradation of methanol. The photodegradation experiments were carried out in a closed box. UV radiation source was 100 W high-pressure mercury lamp, its wavelength range was 209−450 nm and the peak intensity was 365 nm (model OCRS-I, Kaifeng Hxsei Science Instrument Factory, China). No pure oxygen was supplied because it had enough oxygen for oxidation photodegradation under continuously stirring in atmosphere in previous experiment. Twenty mg of TiO_2/HNTs catalyst was suspended in 5 mL 5 vol % methanol aqueous solution at different pH (4.0, 6.9, and 9.2), which was adjusted by standard buffer solution. The temperature of the reactant solution was maintained below 283 K by a flow of cooling water during the reaction. The amount of CO_2 evolved was analyzed using an online gas chromatography (GC, Agilent 6890). Acetic acid was also used as the model pollutant for UV photocatalysis, 20 mg of the catalyst (TiO_2/HNTs and pure TiO_2) was dispersed in 5 mL of 5 vol % acetic acid aqueous solution, and then investigated by the method as aforementioned.

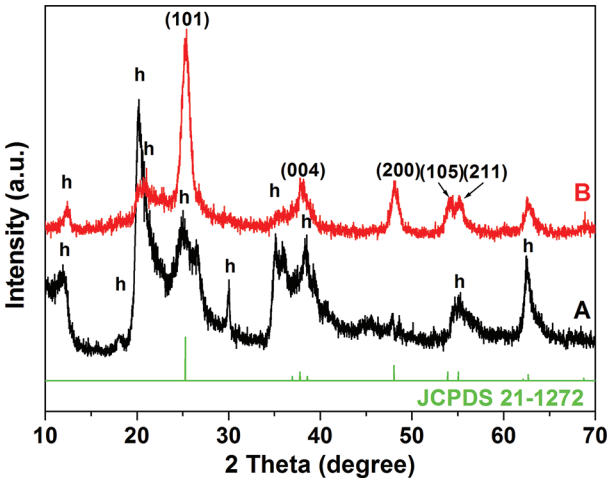

Figure 1. XRD patterns of HNTs (A) and TiO_2/HNTs (B). (h: halloysite).

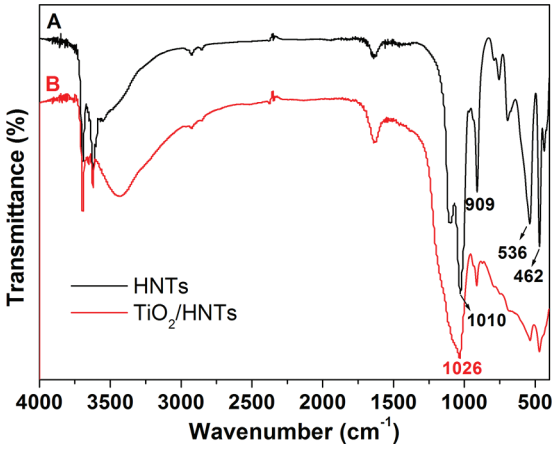

Figure 2. FT-IR spectra of HNTs (A) and TiO_2/HNTs (B).

3. RESULTS AND DISCUSSION

Figure 1 shows the XRD patterns of HNTs (A) and the as-prepared TiO_2/HNTs (B). For the HNTs sample, all of the observed peaks mainly can be indexed to the characteristic peaks of halloysite as shown in Figure 1A.[27] However, the two new peaks at 2θ = 48 and 53.9° and a stronger peak at 2θ = 25.3° can be observed as well as the reduction of the halloysite peaks after the solvothermal treatment. According to JCPDS 21−1272, all of the characteristic peaks of TiO_2 can be ascribed to the (101), (004), (200), (105), (211) planes of anatase structure TiO_2. This indicates that the TiO_2/HNTs were successfully prepared.

The FT-IR spectra of the HNTs and TiO_2/HNTs were used to investigate the composition and structure of the resultant samples. As shown in Figure 2, the TiO_2/HNTs possess some signals due to HNTs, such as the deformations of Al−O−Si and Si−O−Si at 536 and 462 cm^{-1}, respectively, the O−H groups of the inner hydroxyl groups at 909 cm^{-1}. Compared to HNTs, no other characteristic signals are detected in TiO_2/HNTs, but the Si−O broad stretching band at about 1010 cm^{-1} shifts to about 1026 cm^{-1}, which indicates the existence of hydrogen bonding between TiO_2 and outer surfaces of HNTs.[26] Moreover, some properties of HNTs are still preserved after solvothermal

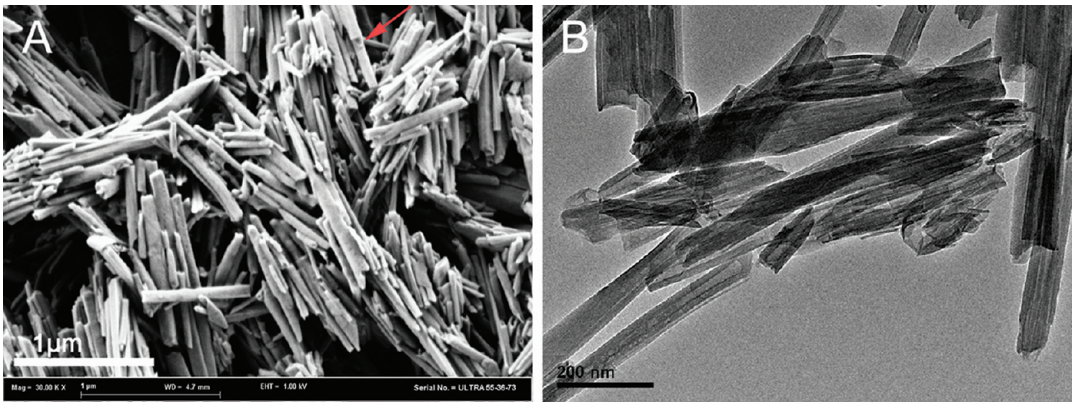

Figure 3. FE-SEM (A) and TEM (B) images of HNTs.

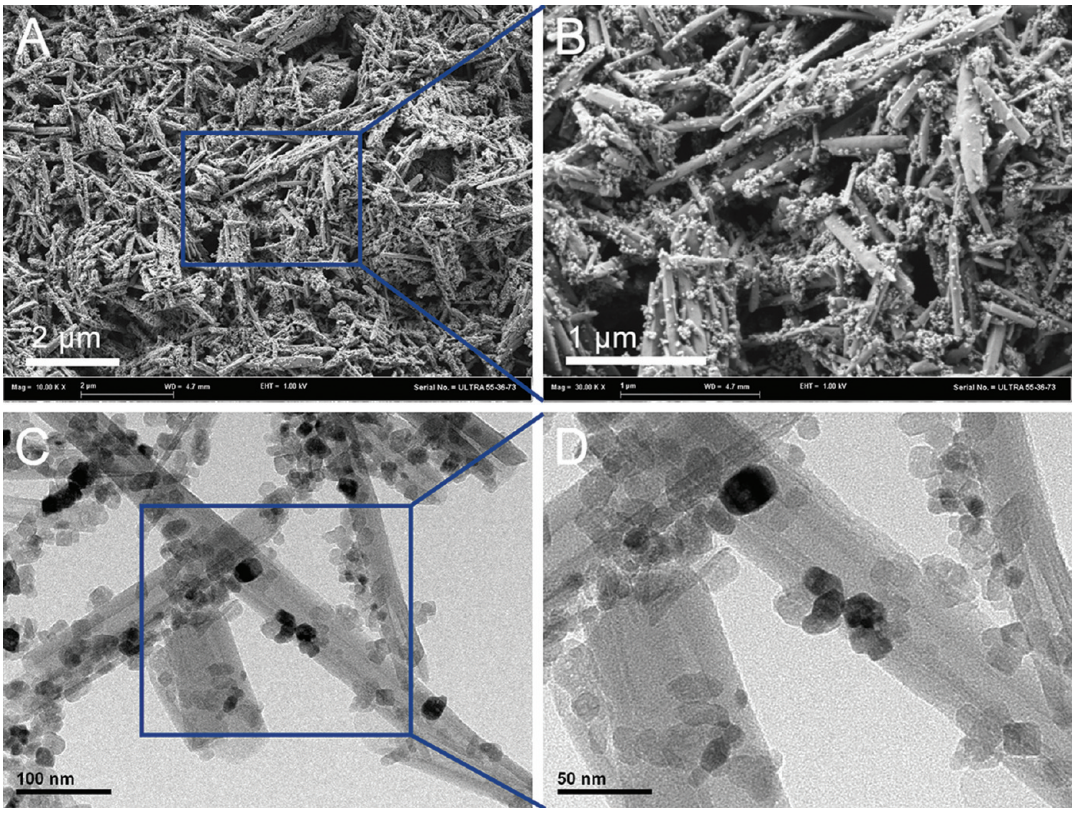

Figure 4. Panoramic FE-SEM (A) and corresponding magnified FE-SEM images (B) of TiO_2/HNTs, TEM (C) and corresponding magnified TEM images (D) of TiO_2/HNTs.

treatment because there is no significant change in the spectrum of HNTs.

The structure and morphology of HNTs were characterized by their corresponding FE-SEM and TEM images. As shown in Figure 3A, the majority of the samples consist of cylindrical tubes 50−70 nm in diameter and 0.5−2 μm in length. HNTs are rather ploydisperse in length. FE-SEM image reveals the empty lumen structure of HNTs (see arrow in Figure 3A), which is consistent with the corresponding TEM image (Figure 3B). Moreover, the empty lumen of HNTs is 15−25 nm in diameter.

A one-step solvothermal method was applied to prepare TiO_2/HNTs. The successful preparation of TiO_2/HNTs was confirmed by their corresponding FE-SEM and TEM images. A large amount of nanoparticles deposited on halloysite nanotubes can be found in Figure 4A, which is in accordance with the TEM results (Figure 4C). The TiO_2 nanoparticles are irregularly dispersed on the surface of halloysite nanotubes, which makes the surface of TiO_2/HNTs become more rough (Figure 4B). In addition, the porosity was also confirmed by the pore analysis based on N_2 adsorption measurement (see Figure S1 in the Supporting Information), which indicates the existence of mesopores and macropores. The BET surface area of HNTs and TiO_2/HNTs are around 38.72 and 30.51 m^2/g, respectively (Table S1 in the Supporting Information). The reduction of the BET surface area of TiO_2/HNTs can be attributed to the deposition of the TiO_2 nanoparticles. The high magnification TEM image (Figure 4D)

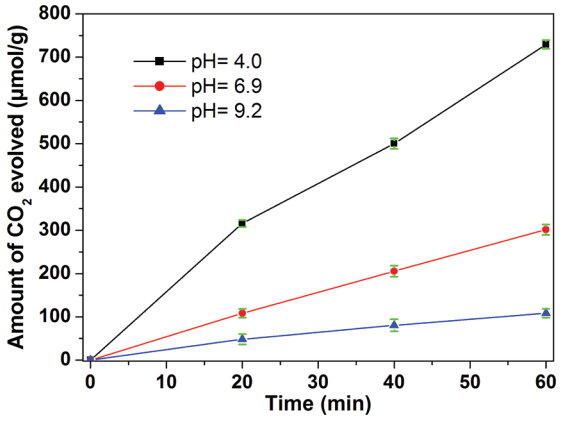

Figure 5. Relationship between the amount of CO_2 evolved and irradiation time for photocatalytic degradation of methanol aqueous solution at various pH.

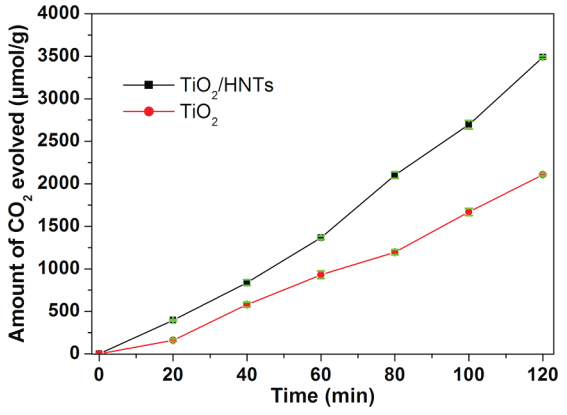

Figure 6. Relationship between the amount of CO_2 evolved and irradiation time for photocatalytic degradation of acetic acid aqueous solution.

of a portion of the TiO_2/HNTs shows that TiO_2 nanoparticles consist of TiO_2 polyhedra with sizes between 5 and 15 nm. The chemical elemental component of the resultant samples was characterized by energy-dispersive X-ray spectrometry (EDS), which indicates the TiO_2/HNTs are composed of the elements Al, Si, Ti, and O (Figure S2 in the Supporting Information).

The photocatalytic activity of TiO_2/HNTs samples was evaluated by the degradation of methanol and acetic acid. Figure 5 shows the amount of CO_2 evolution against irradiation time on photocatalytic degradation of methanol under various pH. After UV irradiation for 1 h, the CO_2 evolution rate reaches 729.37 ± 10.00 μmol h^{-1} g^{-1} under the acidic environment (pH 4.0) (details were shown in Table S2 in the Supporting Information). The value is about 2.42 and 6.72 times higher than that at neutral and alkaline conditions, respectively. According to previous studies, the effect of pH on the photocatalytic reaction is generally attributed to the surface charge of TiO_2 and support.[28−30] As it is know, the surface of TiO_2 catalyst is positively charged at pH values lower than 6.3 and negatively charged at higher pH values due to the point of zero charge (pzc) of TiO_2 is at a pH value of 6.3.[31] Moreover, the surface of HNTs is negatively charged above pH 2.4, thus positively charged molecules can be easily adsorbed on the HNTs and then effectively degraded.[32] Therefore, any charged molecules can be adsorbed on the surface of TiO_2/HNTs at acidic environment, which results in higher photocatalytic activity.

The process of the photocatalytic degradation of methanol can be mainly divided into two steps: (a) The formation of formaldehyde and formic acid, which result from the oxidation of methanol. (b) Photocatalytic degradation of formic acid to produce CO_2 and H_2O. The UV irradiation activates TiO_2 to generate strongly oxidative holes (h_{VB}^+) in valence band and reductive electrons (e_{CB}^-) in conduction band. The h_{VB}^+ can oxidize the methanol directly or react with H_2O to generate a free radical ·OH and H^+, and H^+ subsequently react with the absorbed O_2 to yield ·OH. The free radical ·OH could also oxidize the methanol to form formaldehyde and formic acid, and further oxidize to CO_2 and H_2O (Scheme 1).[33−35]

$$TiO_2 \xrightarrow{h\nu} e_{CB}^- + h_{VB}^+$$

$$h_{VB}^+ + H_2O \rightarrow \cdot OH + H^+$$

$$O_2 + 2H^+ + 3e_{CB}^- \rightarrow \cdot OH + OH^-$$

$$CH_3OH \xrightarrow{\cdot OH \text{ or } h_{VB}^+} HCHO \xrightarrow{\cdot OH \text{ or } h_{VB}^+} HCOOH \xrightarrow{\cdot OH \text{ or } h_{VB}^+} CO_2 + H_2O$$

Higher photocatalytic activity of the TiO_2/HNTs samples was also confirmed by the degradation of acetic acid. As shown in Figure 6, the amount of CO_2 evolution increases with irradiation time for the pure TiO_2 and TiO_2/HNTs samples. However, in the case of TiO_2/HNTs, the CO_2 evolution rate reach around 1744.31 ± 7.63 μmol h^{-1} g^{-1} comparing with the 1053.12 ± 7.23 μmol h^{-1} g^{-1} for pure TiO_2 sample after UV irradiation for 2 h (details were shown in Table S3 in the Supporting Information). The higher CO_2 evolution rate for TiO_2/HNTs sample may be attributed to the adsorptivity of halloysite and the crystalline TiO_2 nanoparticles in which enhance the photocatalytic activity by facilitating the access to the reactive TiO_2.[36] Moreover, the homogeneous dispersion of TiO_2 nanoparticles on HNTs blocks the aggregation of them. Compared the CO_2 evolution rate on the degradation of methanol and acetic acid, a higher degradation rate can be found in the latter case. We speculated that most of active radical (such as ·OH) is consumed to form formaldehyde and formic acid during the degradation of methanol, resulting in the lower rate of CO_2 evolution.

4. CONCLUSION

In summary, a one-step solvothermal method has been developed to prepare the TiO_2/halloysite composite. The as-prepared samples show pH sensibility and high photocatalytic activity on the degradation of methanol which is resulted from the cooperation of the unique structure of halloysite and properties of TiO_2 nanoparticles. Comparing the photocatalytic degradation for methanol and acetic acid, the latter exhibits a higher degradation rate for few radical need to be consumed during the degradation reaction. Therefore, the combination of the photocatalytic property of TiO_2 and the adsorptivity of halloysite endowed this material with a bright perspective in purification of wastewater.

■ ASSOCIATED CONTENT

Supporting Information. Additional figures and tables (PDF). This material is available free of charge via the Internet at http://pubs.acs.org.

■ AUTHOR INFORMATION

Corresponding Author

*Tel: +86 571 86843527. E-mail: polymer_jiang@hotmail.com (G.J.); chenwxg@yahoo.com.cn (W.C.).

■ ACKNOWLEDGMENT

This work was financially supported by the National Natural Science Foundation of China (51133006), the Qianjiang Talents Project of Zhejiang Province (2010R10023), the Scientific Research Foundation for the Returned Overseas Chinese Scholars, the State Education Ministry (1001603-C), the Natural Science Foundation of Zhejiang Province (Y4100045) and the Program for Changjiang Scholars and Innovative Research Team in University (PCSIRT: 0654).

■ REFERENCES

(1) Fujishima, A.; Honda, K. *Nature* **1972**, *238*, 37–38.
(2) Yu, H. T.; Quan, X.; Chen, S.; Zhao, H. M. *J. Phys. Chem. C* **2007**, *111*, 12987–12991.
(3) Aluri, G. S; Motayed, A.; Davydov, A. V; Oleshko, V. P; Bertness, K. A; Sanford, N. A; Rao, M. V. *Nanotechnology* **2011**, *22*, 295503.
(4) Li, H.; Zhou, Y.; Lv, C. X.; Dang, M. M. *Mater. Lett.* **2011**, *65*, 1808–1810.
(5) Xu, X. J.; Tang, C. C.; Zeng, H. B.; Zhai, T. Y.; Zhang, S. Q.; Zhao, H. J.; Bando, Y.; Golberg, D. *ACS Appl. Mater. Interfaces* **2011**, *3*, 1352–1358.
(6) Yu, J. G.; Liu, W.; Yu, H. G. *Cryst. Growth Des.* **2008**, *8*, 930–934.
(7) Pathak, P.; Meziani, M. J.; Li, Y.; T. Cureton, L. T.; Sun, Y. P. *Chem. Commun.* **2004**, 1234–1235.
(8) Hensel, J.; Wang, G. M.; Li, Y.; Zhang, J. Z. *Nano Lett.* **2010**, *10*, 478–483.
(9) Nguyen-Phana, T. D.; Kima, E. J.; Hahnb, S. H.; Kimc, W. J.; Shin, E. W. *J. Colloid Interface Sci.* **2011**, *356*, 138–144.
(10) Jiang, G. D.; Lin, Z. F.; Zhu, L. H.; Ding, Y. B.; Tang, H. Q. *Carbon* **2010**, *48*, 3369–3375.
(11) Wang, S.; Wang, T.; Chen, W. X.; Hori, T. *Chem. Commun.* **2008**, *32*, 3756–3758.
(12) Zon, W. W.; Zhang, J. L.; Chen, F. *Mater. Lett.* **2010**, *64*, 1710–1712.
(13) Jiang, G. H.; Zheng, X. Y.; Wang, Y.; Li, T. W.; Sun, X. K. *Powder Technol.* **2011**, *207*, 465–469.
(14) Jiang, Z. Z.; Wang, Z. B.; Chu, Y. Y.; Gu, D. M.; Yin, G. P. *Energy Environ. Sci.* **2011**, *4*, 2558–2566.
(15) Peng, T. Y.; Zeng, P.; Ke, D. N.; Liu, X. J; Zhang, X. H. *Energy Fuels* **2011**, *25*, 2203–2210.
(16) Li, S. K.; Huang, F. Z.; Wang, Y; Shen, Y. H.; Qiu, L. G.; Xie, A. J.; Xu, S. J. *J. Mater. Chem.* **2011**, *21*, 7459–7466.
(17) Xuan, S. H.; Jiang, W. Q.; Gong, X. L.; Hu, Y.; Chen, Z. Y. *J. Phys. Chem. C* **2009**, *113*, 553–558.
(18) Zhu, C. Z.; Guo, S. J.; Wang, P.; Xing, L.; Fang, Y. X.; Zhai, Y. M.; Dong, S. J. *Chem. Commun.* **2010**, *46*, 7148–7150.
(19) Zhao, H.; Yang, J.; Wang, L.; Tian, C. G.; Jiang, B. J.; Fu, H. G. *Chem. Commun.* **2011**, *47*, 2014–2016.
(20) Li, Q.; Guo, B. D.; Yu, J. G.; Ran, J. R.; Zhang, B. H.; Yan, H. J.; Gong, J. R. *J. Am. Chem. Soc.* **2011**, *133*, 10878–10884.
(21) Zhai, R.; Zhang, B.; Liu, L.; Xie, Y. D.; Zhang, H. Q.; Liu, J. D. *Catal. Commun.* **2010**, *12*, 259–263.
(22) Vergaro, V.; Abdullayev, E.; Lvov, Y. M.; Zeitoun, A.; Cingolani, R.; Rinaldi, R.; Leporatti, S. *Biomacromolecules* **2010**, *11*, 820–826.
(23) Reshmi, R.; Sanjay, G.; Sugunan, S. *Catal. Commun.* **2006**, *7*, 460–465.
(24) Wang, J. H.; Zhang, X.; Zhang, B.; Zhao, Y. F.; Zhai, R.; Liu, J. D.; Chen, R. F. *Desalination* **2010**, *259*, 22–28.
(25) Tierrablanca, E.; Romero-García, J.; Roman, P.; Cruz-Silva, R. *Appl. Catal. A: Gen.* **2010**, *381*, 267–273.
(26) Papoulis, D.; Komarneni, S.; Nikolopoulou, A.; Tsolis-Katagas, P.; Panagiotaras, D.; Kacandes, H. G.; Zhang, P.; Yin, S.; Sato, T.; Katsuki, H. *Appl. Clay Sci.* **2010**, *50*, 118–124.
(27) Wang, L.; Chen, J. L.; Zhu, Z. H.; Rudolph, V. *Energy Fuels* **2011**, *25*, 3408–3416.
(28) Jiang, G. H.; Wang, R. J.; Jin, H.; Wang, Y.; Sun, X. K.; Wang, S.; Wang, T. *Powder Technol.* **2011**, *212*, 284–288.
(29) Robert, D.; Dongui, B.; Weber, J. V. *J. Photochem. Photobiol., A: Chem* **2003**, *156*, 195–200.
(30) Lin, W. C.; Yang, W. D.; Huang, I. L.; Wu, T. S.; Chung, Z. J. *Energy Fuels* **2009**, *23*, 2192–2196.
(31) Evgenidou, E.; Fytianos, K.; Poulios, I. *J. Photochem. Photobiol., A: Chem.* **2005**, *175*, 29–38.
(32) Abdullayev, E.; Price, R.; Shchukin, D.; Lvov, Y. *ACS Appl. Mater. Interfaces* **2009**, *1*, 1437–1443.
(33) Chiarello, G. L.; Ferri, D.; Selli, E. *J. Catal.* **2011**, *280*, 168–177.
(34) Goldstein, S.; Behar, D.; Rabani, J. *J. Phys. Chem. C* **2008**, *112*, 15134–15139.
(35) Du, Y. K.; Rabani, J. *J. Phys. Chem. B* **2003**, *107*, 11970–11978.
(36) Guo, J. J.; Zhu, S. M.; Chen, Z. X.; Li, Y.; Yu, Z. Y.; Liu, Q. L.; Li, J. B.; Feng, C. L.; Zhang, D. *Ultrason. Sonochem.* **2011**, *18*, 1082–1090.